PAIR PRODUCTION OF SCALAR TOP QUARKS IN e^+e^- COLLISIONS AT ILC

A. Bartl[a,b] *, W. Majerotto[c] †, K. Mönig[d] ‡, A. N. Skachkova[e] §, N. B. Skachkov[e] ¶

[a] *University of Vienna, Faculty of Physics, 1090 Vienna, Boltzmanngasse 5, Austria.*
[b] *AHEP Group, Instituto de Fisica Corpuscular - C.S.I.C., Universidad de Valencia, Edificio Institutos de Investigacion, Apt. 22085, E-46071 Valencia, Spain*
[c] *Institute for High Energy Physics (HEPHY Vienna), Nikolsdorfergasse 18, A-1050 Vienna, Austria.*
[d] *DESY, Platanenallee 6, D-15738 Zeuthen, Germany.*
[e] *JINR, Joliot-Curie 6, 141980 Dubna, Moscow region, Russia.*

Abstract

We study the pair production of scalar top quarks (stop, $\tilde{t}_1$) in e^+e^- collisions with the subsequent decay of the top squarks into b-quarks and charginos $\tilde{t}_1 \to b\tilde{\chi}_1^{\pm}$. We simulate this process by using PYTHIA6 for a beam energy $2E^e_{beam} = \sqrt{s_{ee}} = 500$ GeV. A set of criteria for physical variables is proposed which provides a good separation of stop signal events from top quark pair production which is the main background. These criteria allow us to reconstruct the mass of the top squark with two years of ILC running provided that the neutralino mass is known.

1 Introduction.

The scalar top quark, the bosonic partner of the top quark, has attracted much attention as it is expected to be the lightest colored suppersymmetric (SUSY) [1] particle. $\tilde{t}_L$ and $\tilde{t}_R$, the supersymmetric partners of the left-handed and right-handed top quarks, mix and the resultant two mass eigenstates $\tilde{t}_1$ and $\tilde{t}_2$, can have a large mass splitting. It is even possible that the lighter eigenstate $\tilde{t}_1$ could be lighter than the top quark itself [2], [3].

Experimental searches for top squarks were performed at LEP and Tevatron. The present status of these experimental efforts is reflected in Figure 1, taken from [4], which shows that the mass of the stop is higher than 141 GeV for a mass difference between the stop and the lightest neutralino of about 50-70 GeV (see Fig.1). These searches will continue at LHC and ILC [6], [7].

This Note is the continuation of our previous Note where we have considered stop pair production in photon-photon collisions [8]. In what follows we study the reaction

$$e^+ + e^- \to \tilde{t}_1 + \bar{\tilde{t}}_1. \tag{1}$$

Among the possible $\tilde{t}_1$-decay channels within the MSSM (see [9] for details), we focus on the decay $\tilde{t}_1 \to b\tilde{\chi}_1^{\pm}$ followed by the two-body chargino decay $\tilde{\chi}_1^{\pm} \to \tilde{\chi}_1^0 W^{\pm}$, where one of the

* **e-mail**: bartl@univie.ac.at
† **e-mail**: majer@qhepu3.oeaw.ac.at
‡ **e-mail**: klaus.moenig@desy.de
§ **e-mail**: Anna.Skachkova@cern.ch
¶ **e-mail**: skachkov@jinr.ru

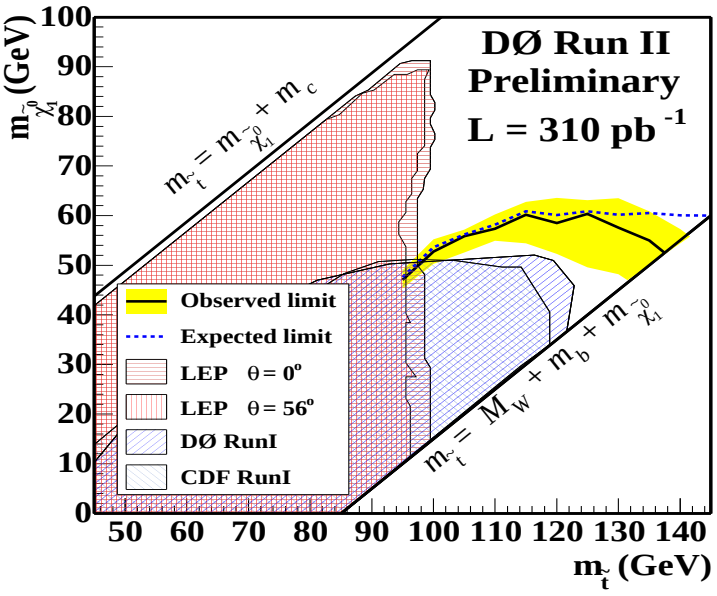

Figure 1: *The current exclusion limits, obtained at Tevatron and LEP, based on the search in the* $\tilde{t} \to c\chi_1^0$ *channel (taken from [4]).*

W's decays hadronically, $W \to q_i\bar{q}_j$, and the other one leptonically, $W \to \mu\nu_\mu$ [10][1]. The final state of this signal process, shown in the left-hand plot of Fig.2, contains two b-jets and two (or more) jets (originating from the decay of one W boson) and a hard muon plus a neutrino (from the decay of the other W) and two neutralinos:

$$e^+e^- \to \tilde{t}_1\bar{\tilde{t}}_1 \to b\bar{b}\tilde{\chi}_1^+\tilde{\chi}_1^- \to b\bar{b}W^+W^-\tilde{\chi}_1^0\tilde{\chi}_1^0 \to b\bar{b}q_i\bar{q}_j\mu\nu_\mu\tilde{\chi}_1^0\tilde{\chi}_1^0. \tag{2}$$

The main background process is top quark pair production with the subsequent decay $t \to bW^\pm$ (for W's we use the same decay channels as in the stop case):

$$e^+e^- \to t\bar{t} \to b\bar{b}W^+W^- \to b\bar{b}q_i\bar{q}_j\mu\nu_\mu. \tag{3}$$

The only difference between the final states of stop and top production (see right-hand plot of Fig.2) is that in stop pair production there are two neutralinos which are undetectable. In the present paper we consider only top pair production as background. The analysis of the

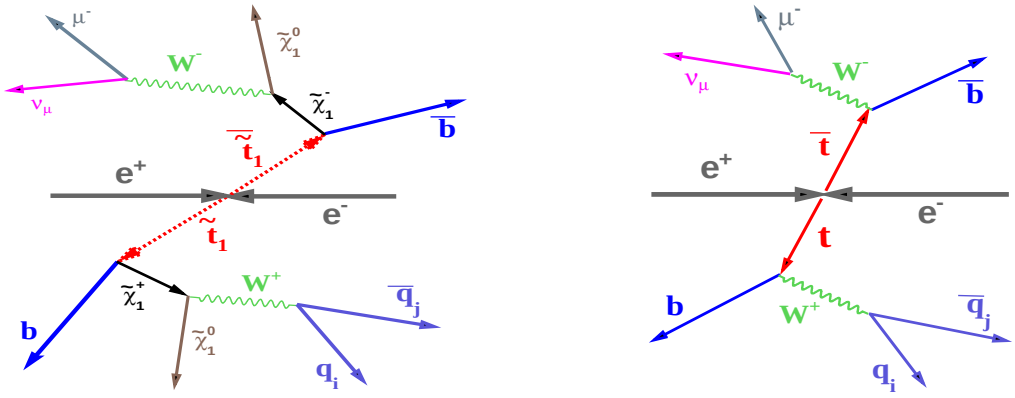

Figure 2: *Left is the stop signal event diagram, Right is the top background diagram.*

processes (2) and (3) is done on the basis of Monte Carlo samples of the corresponding events.

[1] The process $e^+e^- \to \tilde{t}_1 + \bar{\tilde{t}}_1$ with the subsequent decay $\tilde{t}_1 \to c\tilde{\chi}_1^0$ was considered in [11] –[13].

Two programs PYTHIA6.1 [14] and CIRCE1 [15] were used. The top background was also simulated with PYTHIA6.1. The program CIRCE1 was used for the simple parameterizations of the beam spectra involved in processes (1) and (3) to account for the effects of beamstrahlung. The energy of the beams was chosen as $2E^e_{beam} = \sqrt{s_{ee}} = 350$, 400, 500, 800, 1000 GeV.

In Section 2 we give the set of MSSM parameters used in our study.

In Section 3 we discuss some general characteristics of the signal process $e^+e^- \to \tilde{t}_1\bar{\tilde{t}}_1$ and the main background $e^+e^- \to t\bar{t}$. Subsection 3.1 deals with the reconstruction of the invariant mass of the two-quark system stemming from the W boson decay as well as with the reconstruction of the invariant mass of the corresponding two-jet system. Three cuts, applied to select signal stop and background top events, are presented in subsection 3.2. Further subsections include kinematic distributions for the produced stop quarks, b-jets, missing energy, total visible energy, and the scalar sum of the transverse momenta of all visible particles in the event. We always compare them in detail with those of top pair production. In subsection 3.6 we present the values of the signal-to-background ratios (S/B) which may be reached with the three cuts. We also consider the differences between the distributions of the kinematic variables presented in this Section for stop pair production and top pair production. They can be used for further separation of the signal events from the background if more data are available.

In Section 4 we discuss how to discriminate between the signal muons produced in W boson decays and those stemming from hadron decays in the same events.

The following two Sections deal with the invariant mass distributions. In Section 5 we demonstrate that the invariant masses of all final-state hadronic jets and of all final jets plus the signal muon, as well as the missing mass, are good tools for separating the signal from the top background.

In Section 6 we show that the invariant mass of one b-jet and the other two $non-b$-jets (from W decay) allows one to reconstruct the mass of the scalar top quark provided that the neutralino mass is known.

In Section 7 we show the behaviour of distributions of the invariant variables described in Sections 3.5, 5 and 6 for the case of a different stop mass.

Section 8 contains some conclusions.

2 MSSM parameters and cross section.

The scalar top quark system is described by the mass matrix (in the $\tilde{t}_L - \tilde{t}_R$ basis) [2], [16]

$$\begin{pmatrix} M^2_{\tilde{t}_{LL}} & M^2_{\tilde{t}_{LR}} \\ M^2_{\tilde{t}_{RL}} & M^2_{\tilde{t}_{RR}} \end{pmatrix} \tag{4}$$

with

$$M^2_{\tilde{t}_{LL}} = M^2_{\tilde{Q}} + (\frac{1}{2} - \frac{2}{3}sin^2\Theta_W)cos2\beta M^2_Z + M^2_t, \tag{5}$$

$$M^2_{\tilde{t}_{RR}} = M^2_{\tilde{U}} + \frac{2}{3}sin^2\Theta_W cos2\beta M^2_Z + M^2_t, \tag{6}$$

$$M^2_{\tilde{t}_{RL}} = (M^2_{\tilde{t}_{LR}})^* = M_t(A_t - \mu^* cot\beta). \tag{7}$$

The mass eigenvalues are given by

$$M^2_{\tilde{t}_{1,2}} = \frac{1}{2}\left[(M^2_{\tilde{t}_{LL}} + M^2_{\tilde{t}_{RR}}) \mp \sqrt{(M^2_{\tilde{t}_{LL}} + M^2_{\tilde{t}_{RR}}) + 4|M^2_{\tilde{t}_{LR}}|}\right] \tag{8}$$

with the mixing angle

$$cos\theta_{\tilde{t}} = \frac{-M^2_{\tilde{t}_{LR}}}{\sqrt{|M^2_{\tilde{t}_{LR}}|^2 + (M^2_{\tilde{t}_1} - M^2_{\tilde{t}_{LL}})^2}} \tag{9}$$

$$sin\theta_{\tilde{t}} = \frac{M^2_{\tilde{t}_{LL}} - M^2_{\tilde{t}_1}}{\sqrt{|M^2_{\tilde{t}_{LR}}|^2 + (M^2_{\tilde{t}_1} - M^2_{\tilde{t}_{LL}})^2}} \tag{10}$$

In what follows we shall consider only one particular choice of the MSSM parameters that are defined, in the notations of PYTHIA6, in the following way:

- $M_{\widetilde{Q}} = 270$ GeV;
- $M_{\widetilde{U}} = 270$ GeV;
- $A_t = -500$ GeV (top trilinear coupling);
- $tan\beta = 5$;
- $\mu = -370$ GeV;
- $M_1 = 80$ GeV;
- $M_2 = 160$ GeV.

Note that in PYTHIA6 $M_{\widetilde{Q}}$ corresponds to $M_{\widetilde{t}_L}$ (left squark mass for the third generation) and $M_{\widetilde{U}}$ corresponds to $M_{\widetilde{t}_R}$. These parameters give $M_{\widetilde{t}_1} = 167.9$ GeV, $M_{\chi_1^+} = 159.2$ GeV and $M_{\chi_1^0} = 80.9$ GeV. This value of $M_{\widetilde{t}_1}$ is rather close to the mass of the top quark $M_{top} = 170.9 \pm 1.8$ GeV [17]. Therefore one expects a rather large contribution from the top background, which means that the choice of this value of the stop mass makes the analysis most difficult. Finding a suitable set of cuts separating stop and top events will be crucial.

In general, the cross section for stop pair production at a fixed energy depends on the mass of the stop quark and the mixing angle $\theta_{\tilde{t}}$. Since the couplings of the Z^0 to the left and right components of the stop are different, the cross sections depend significantly on the beam polarizations (see [9], [10], [21]). By chosing the appropriate longitudinal beam polarizations it is possible to enchance the cross sections. For example, for an electron beam with 90% left polarization the cross section would be larger than the unpolarised cross section by approximately 40%, for cos $\theta_{\tilde{t}}$ = - 0.81 corresponding to the parameters given above. If in addition the positron beam has 60% right polarization, then the cross section is enhanced by approximately a factor of 2 compared to the unpolarized cross section. We note that a rather precise determination of the stop mixing angle $\theta_{\tilde{t}}$ is possible by measuring the left-right asymmetry. The cross section for top pair production has also a characteristic dependence on the beam polarizations [21]. For example, the polarization of both beams leads to an increase of the cross section by about a factor of 1.5.

3 Distributions of kinematic variables in stop and top production.

In this Section we present various plots of distributions for different physical variables based on $2.5 \cdot 10^4$ stop pair production events generated by CIRCE1 and PYTHIA6.1 and weighted by the electron-positron luminosity. Analogous plots are also given for 10^6 generated background top events.

The next Fig.3 **a)** demostrates the total energy spectrum of the electron and positron beams, which is expected after taking into account beamstrahlung and other beam interaction effects (see, for instance [22]). Fig.3 **b)** shows the correlations of the beam fractions $y_i = E^i/E^i_{beam}$ (i=e^+, e^-) of the colliding electron and positron beams.

To find the jets we used the subroutine PYCLUS of PYTHIA with the distance measure used in the "Durham algorithm". The parameters of this jetfinder are chosen such that the number of jets is exactly four. Technically, b-jets are defined as jets that contain at least one B-hadron. Their decay may be identified by the presence of a secondary vertex [18].

Let us also mention that separate stop and top event samples were generated without and with cuts. This shows the effect of the cuts.

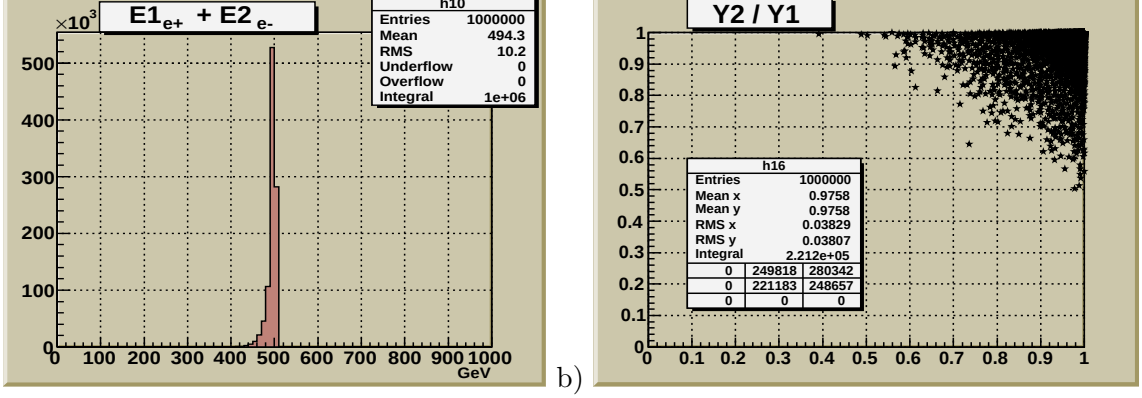

Figure 3: **a)** *total beam energy spectrum,* **b)** *beam fractions correlations*

3.1 Jet distributions from W decay.

In this subsection we present some plots that were obtained without cuts. In addition to the two b-jets there are also, according to the decay chain (2), two jets due to the decay of one W boson into two quarks $W \to q_i + \bar{q}_j$ (see Fig.2).

Figure 4 shows the spectrum of the invariant mass $M_W = M_{inv}(quark1 + quark2)$ reconstructed from the vectorial sum of 4-momenta of these two quarks. We use W^* to denote a virtual W boson. Plot **a)** is for stop pair production, plot **b)** is for top production.

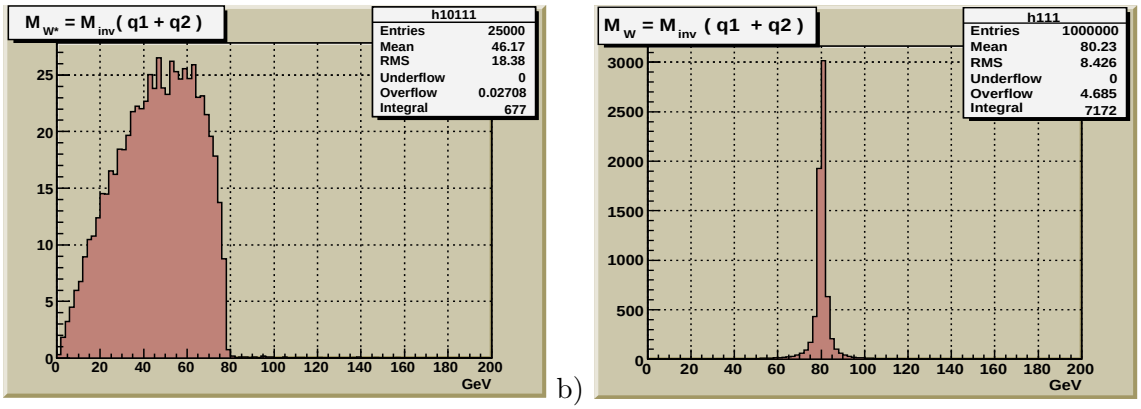

Figure 4: *The invariant mass of two quarks $M_W = M_{inv}(quark1 + quark2)$, reconstructed from the vectorial sum of 4-momenta of two quarks that are produced in $W \to q_i + \bar{q}_j$ decay.* **a)** *stop pair production;* **b)** *top pair production.*

In plot **a)** of Fig.4 one clearly sees the virtual nature of the W boson in the stop pair production case. Hence, in the stop case the invariant mass of two quarks produced in the decay of the virtual W boson (W^*) is smaller than the mass of a real W boson. In top production (see plot **b)** of Fig.4) there is a peak in the invariant mass distribution at the mass value of the real W boson.

Figure 5 shows the corresponding plots at the jet level. The invariant mass in plot **a)** is built of "all-non-b-jets" (or, shortly, "$JETS_{W^*}$") [2]. One can see from plot **a)** that in the stop case the peak position is shifted to the left and a long tail for higher invariant masses appears. As seen from plot **b)**, in the top case at the jet level the position of the W-peak remains at the same value (with a high precision) of M_W as in plot **b)** of Fig.4, except for a shift in the mean value. From comparison of plots **a)** and **b)** of Fig.5 we conclude that the cut $M_{inv}(all - non - b - jets) \leq 70$ GeV allows the elimination of this tail and a big amount of the top background.

[2]There are two jets with our choice of the PYCLUS jetfinder parameters

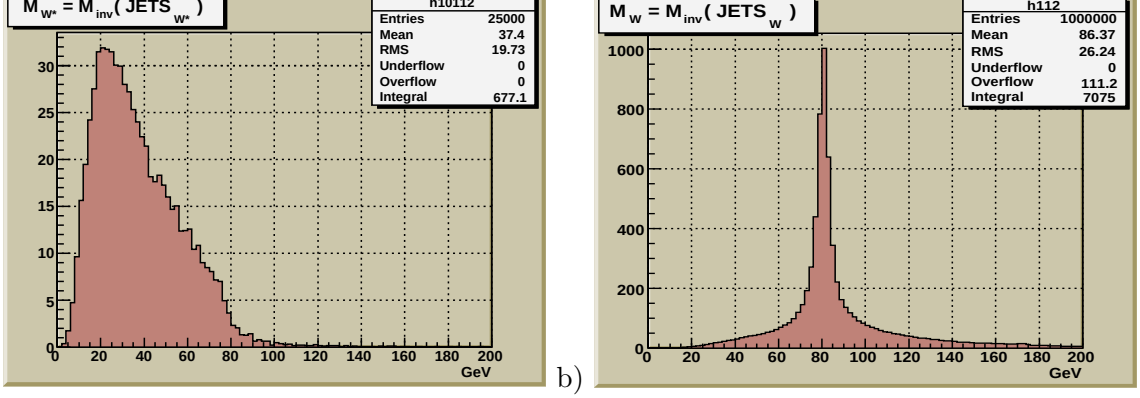

Figure 5: *Number of generated events versus the reconstructed invariant mass of "all-non-b-jets".* **a)** *stop pair production;* **b)** *top pair production.*

3.2 The cuts.

Starting with this subsection we shall present the signal and background distributions which are obtained with the following set of cuts:

- there must be at least two b-jets in an event:

$$N_{b-jets} \geq 2; \tag{11}$$

- the invariant mass of "all-non-b-jets" in an event must be smaller than 70 GeV:

$$M_{inv}(all - non - b - jets) \leq 70\ GeV; \tag{12}$$

- the invariant mass of each b-jet must be smaller than 10 GeV:

$$M_{b-jet} \leq 10\ GeV. \tag{13}$$

b-jets produced in the top decay are much more energetic than b-jets produced in the stop decay, see subsection 3.4.

3.3 Distributions in stop events.

We first give in Table 1 the cross sections and the numbers of events corresponding to the luminosity of 200 fb^{-1} per year for stop pair production and top pair production for different c.m.s. energies.

Table 1: Before the cuts

$2E^e_{beam} = \sqrt{s_{ee}}$ $[GeV]$	$\sigma^{e^+e^-}_{stop}$ $[fb]$	$N^{events}_{stop}/year$	$\sigma^{e^+e^-}_{top}$ $[fb]$	$N^{events}_{top}/year$
350	0.29	58	13.76	2752
400	1.89	378	38.80	7761
500	3.39	677	35.93	7187
800	2.73	546	17.35	3472
1000	1.42	283	11.67	2348

In Table 2 and the following we present only those signal stop and background top events which have passed the imposed cuts (11) -(13) as defined above. In Table 2 we give the corresponding cross sections and the expected numbers of events per year.

In what follows we shall present the distribution plots only for the energy $2E^e_{beam} = \sqrt{s_{ee}} =$ 500 GeV. Due to the 4-momentum conservation in the c.m.s. the produced stops shall have the same energy $E_{\tilde{t}_1}(\equiv E_{stop}) = 250$ GeV and fly back–to–back.

Table 2: After the cuts

$2E^{e}_{beam} = \sqrt{s_{ee}}$ $[GeV]$	$\sigma^{e^+e^-}_{stop}$ $[fb]$	$N^{events}_{stop}/year$	$\sigma^{e^+e^-}_{top}$ $[fb]$	$N^{events}_{top}/year$
350	0.10	21	$3.60 * 10^{-2}$	7
400	0.74	148	$7.46 * 10^{-2}$	14
500	1.38	273	$4.45 * 10^{-2}$	8
800	1.02	203	$9.93 * 10^{-3}$	2
1000	0.11	22	$4.11 * 10^{-3}$	0

Figure 6 shows two kinematic distributions characteristic of the produced stop pair system, i.e., the distributions of its transverse momentum (plot **a)**) $PT_{\tilde{t}_1} (\equiv PT_{stop})$ and its polar angle (see plot **b)** $\theta_{\tilde{t}_1} (\equiv THETA_{stop})$ (all in e^+e^- c.m.s.). As can be seen in Fig.5 **a)** the stop transverse momentum $PT_{\tilde{t}_1} (\equiv PT_{stop})$ spectrum begins from $PT_{\tilde{t}_1} = 50$ GeV and has a peak near the kinematical limit.

a) 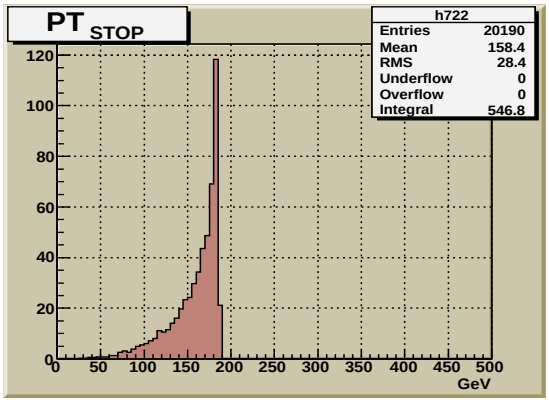

b) 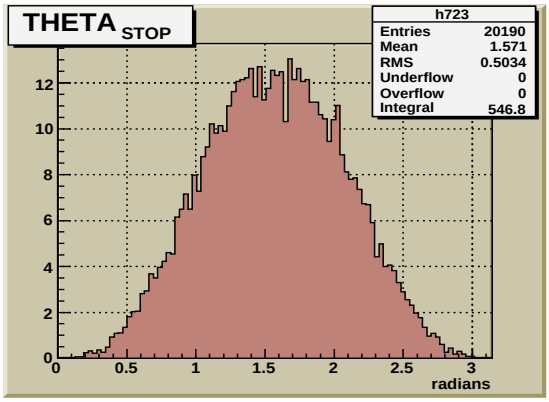

Figure 6: **a)** *Stop transverse momentum* $PT_{\tilde{t}_1} (\equiv PT_{stop})$ *spectrum;* **b)** *Stop polar angle* $\theta (= THETA_{stop})$ *spectrum.*

In Fig.6 and the following figures the vertical axis show the number of stops and antistops produced per year ($= 10^7$ sec) in each bin. Taking the integral of the distributions and dividing its value by two (there is one stop-antistop pair in each event) one can get the total number of events expected per year for the applied cuts. These numbers are shown as "Integral" values within the statistical frames in the right upper corners of the plots.

3.4 *b*-quark and *b*-jet distributions in stop and top production.

In the case of stop decay into a *b*-quark and a chargino, $\tilde{t}_1 \to b\tilde{\chi}^{\pm}_1$, the jets produced in *b*-quark hadronization are observable objects. Their features are interesting from the viewpoint of experimentally distinguishing the stop signal events from the top background.

Plot **a)** (for stop pair production) and plot **b)** (for top pair production) of Fig.7 show the distributions of the energy E_b of the *b*- and $\bar{b}$-quarks (we do not distinguish them in what follows) produced in the decay $\tilde{t}_1 \to b\tilde{\chi}^{\pm}_1$. Both spectra begin at $E_b \geq 4$ GeV (corresponding to the b-quark mass) but look very different. The b-quark energy spectrum in stop production goes up to $E_b \approx 21$ GeV, whereas the corresponding spectrum in top production is much harder and extends up to $E_b \approx 170$ GeV. The mean values of the b-quarks energy are about 13 GeV and 63 GeV in stop and top production respectively. It means that in the stop case (see plot **a)**) the b-quark takes a smaller part of the stop energy $E_{\tilde{t}_1} = 250$ GeV.

Figure 8 shows the transverse momentum PT_b spectra of *b*-quarks for stop (plot **a)**) and top (plot **b)**) production. Comparing plot **a)** of Fig.8 with plot **a)** in Fig.6, one can see that in stop pair production the *b*-quarks also take only a small fraction of the transverse momentum of the

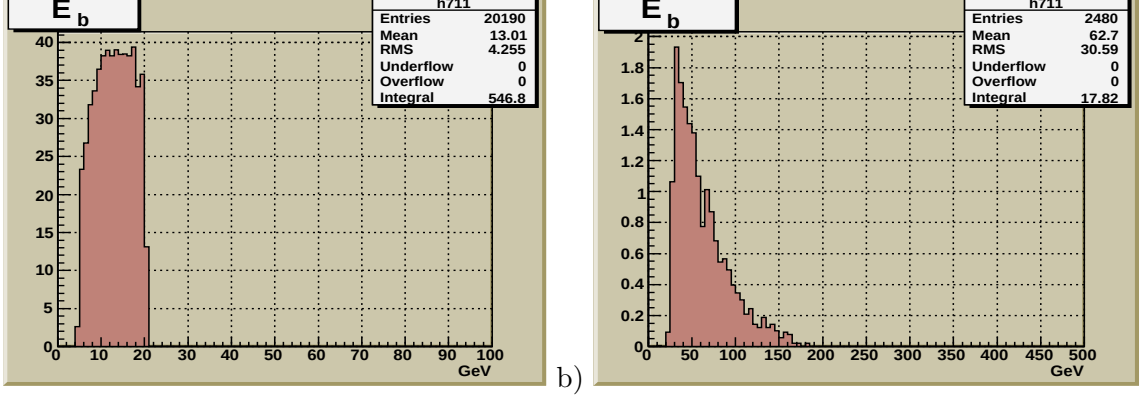

Figure 7: *b- and $\bar{b}$-quark energy spectra.* **a)** *stop pair production;* **b)** *top pair production.*

parent stops. The shapes of the PT_b spectra of these b-quarks are similar to the E_b spectra. This means that in the stop decay the transverse component of the b-quark momentum is larger than the longitudinal component.

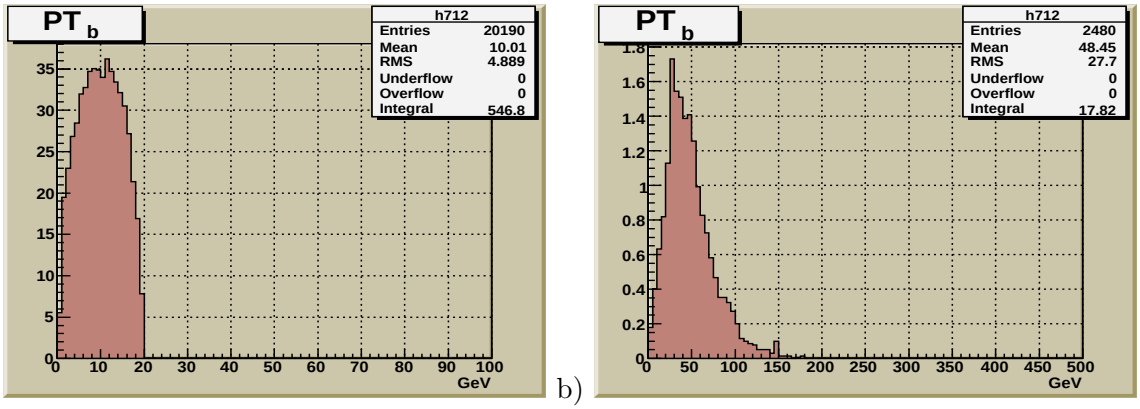

Figure 8: *b- and $\bar{b}$-quark PT spectra.* **a)** *stop pair production;* **b)** *top pair production.*

The kinematic distributions of the b-quarks in the top decay are quite different. As seen from plots **b)** of Fig.7 and Fig.8, the b-quarks produced in the top decays are very energetic and have large transverse momenta. This difference from the stop decay is easily understandable. The stop decays into a heavy chargino, while the top decays into a real W boson whose mass is only half of the mass of the chargino $M_{\chi_1^\pm}$. Therefore, the b-quarks produced in top decays have a larger phase space than the b-quarks produced in stop decays.

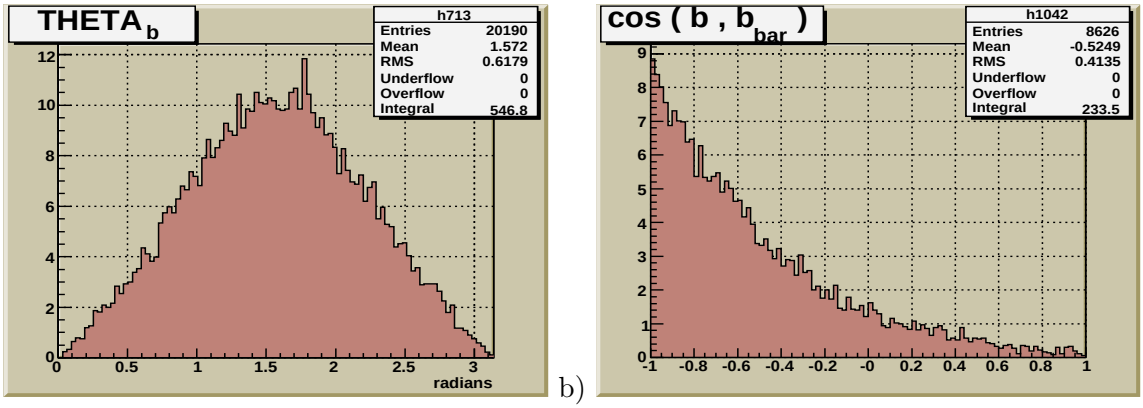

Figure 9: **a)** *b- and $\bar{b}$-quark polar angle θ_b distribution in stop production;* **b)** *$cos(b, \bar{b})$ distribution in stop production.*

The polar angle $\theta_b(\equiv THETA_b)$ distribution of the b-quarks in stop production is presented in plot **a)** of Fig.9. Plot **b)** of Fig.9 contains the $cos(b,\bar{b})$ distribution, where $cos(b,\bar{b})$ is the cosine of the opening angle between the 3-momenta of the b- and $\bar{b}$-quarks produced in the same stop event. It demonstrates that most of the b- and $\bar{b}$-quarks move approximately in the opposite directions, but a part of them are in the same hemisphere. Thus in the experiment we may expect a similar angular distributions of the corresponding b- and $\bar{b}-jets$ in stop pair production.

As the next step, we take into account b-quark hadronization into a b-jet. Figs.10 and 11 show the energy E_{b-jet} and transverse momentum PT_{b-jet} distributions of the corresponding b-jets. Plots **a)** and **b)** of Fig.10 are for stop and top production, respectively. These plots and the following plots for jets were obtained using the "Durham algorithm" definition of the distance measure implemented in the PYCLUS jetfinder of PYTHIA.

a) 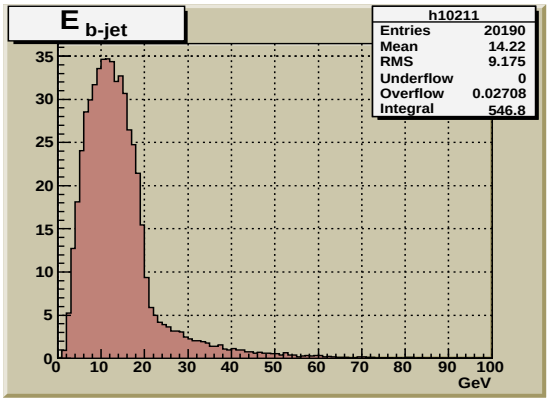

b) 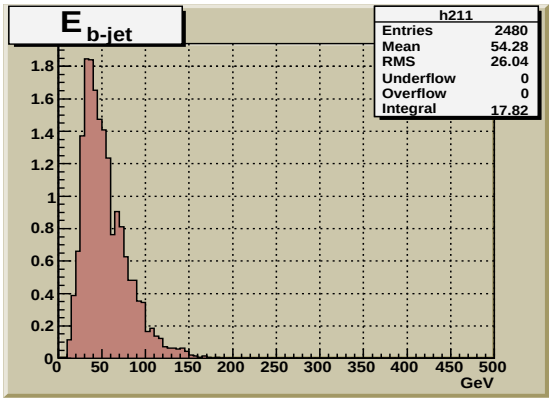

Figure 10: *b-jet energy spectra.* **a)** *stop pair production;* **b)** *top pair production.*

Comparing plots **a)** of Figs.10 and 11 for the b- and $\bar{b}$- jet energy and jet transverse momentum PT_{b-jet} distributions in stop production with the Figs.7 **a)** and 8 **a)**, one observes that the corresponding mean values of the jet energies in Fig.10 are only about 1 GeV higher than those for the quarks. Furthermore, the end points of the energy distributions for the b-jets and $\bar{b}$-jets are somewhat higher than those for the corresponding quarks. There are not very pronounced long tails at higher energies and the energy spectrum begins at smaller values when passing to the jet level. Due to the different kinematics in top production, the mean values of the b-jet and $\bar{b}$-jet energy distributions are about 8 GeV smaller than the mean values of the corresponding b-quark and $\bar{b}$-quark energy distributions (see Fig.7 **b)** and Fig.10 **b)**).

a) 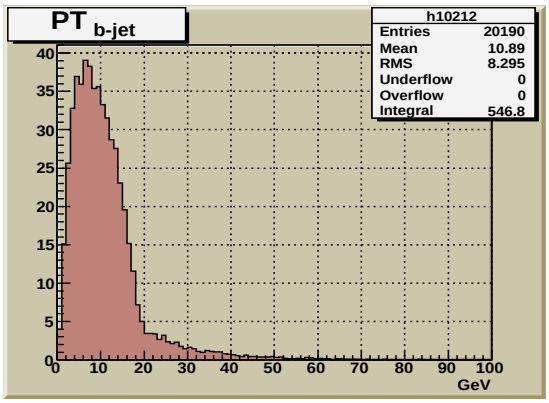

b) 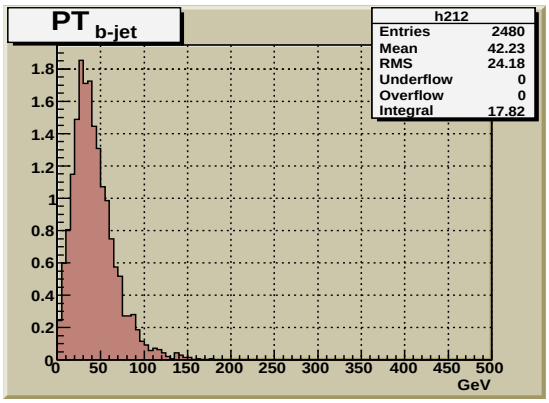

Figure 11: *b-jet PT- spectra.* **a)** *stop pair production;* **b)** *top pair production.*

Figure 11 shows the transverse momentum PT_{b-jet} distributions of the b-jets and $\bar{b}$-jets in stop production (plot **a)**) and top production (plot **b)**). By comparing with Fig.8 for the

corresponding PT distributions at the b-quark level we can see that for stop production there is practically no change of the mean value and the shape except the appearance of not very large tails at high PT. In the case of top production the PT distributions are wider than in the stop production case. The mean values of the PT distributions of b-jets are about 6 GeV smaller than of the b-quarks, but there is no high PT tail as it was in the stop case.

Even after application of the cut (13) the b-jet energy and transverse momentum spectra in top production still remain much harder than those in the stop case. This may suggest to use this cut for top background reduction. Its efficiency will be demonstrated in subsection 3.6.

3.5 Distributions of the total energy deposition and scalar P_T-sum.

In stop pair production the two neutralinos and the energetic neutrino from the W boson decay escape detection. The simulation with PYTHIA6 allows us to estimate the missing energy and the missing transverse momenta that are carried away by these particles. We also take into account the non-instrumented region around the beam pipe given by the polar angle intervals $\Theta < 7^o$ and $\Theta > 173^o$.

The distributions of the total missing energy for stop production and top production are presented in **a)** and **b)** plots of Fig.12, respectively. In stop pair production, see plot **a)** the $E_{miss-tot}$ spectrum starts at 190-200 GeV. In top pair production (plot **b)**), where two neutralinos are not present, the missing energy $E_{miss-tot}$ is much smaller.

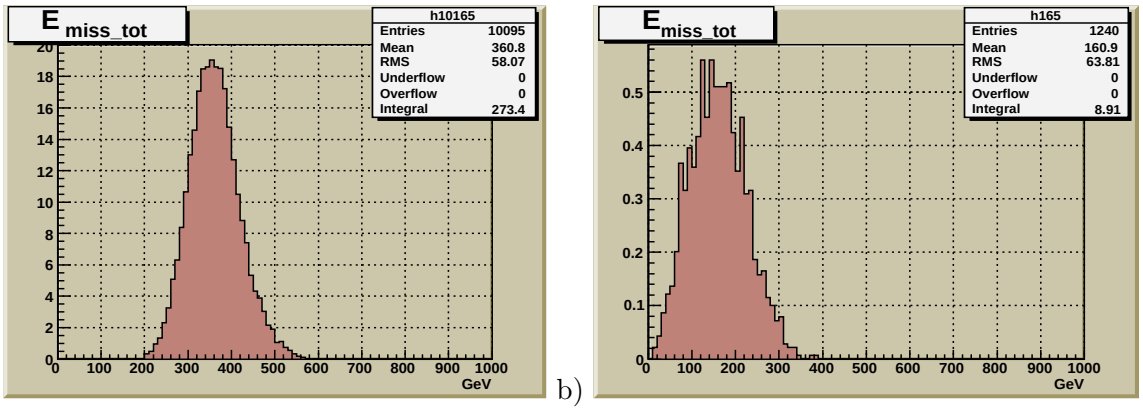

Figure 12: *Missing energy $E_{miss-tot}$ distribution.* **a)** *stop pair production;* **b)** *top pair production.*

Figure 13 shows the distributions of the total energy deposited in the calorimeter ("visible energy") $E_{cal-tot}$ in stop production (plot **a)**) and in top production (plot **b)**). The large missing energy in stop production (Fig.12) is related to the low visible energy (Fig.13), while in top production the low missing energy correlates with the large visible energy. A cut on the total visible energy of approximately $E_{cal-tot} < 180$ GeV [3] would eliminate completely the top background.

Another useful observable is the scalar sum of the moduli of the transverse momenta in an event $PT_{scalsum} = \sum_{i=1}^{n} |PT_i|$, where the sum goes over all detectable particles in the event. Figure 14 shows the distributions of the scalar sum of the transverse momenta for the stop production (plot **a)**) and for top production (plot **b)**). It is seen that the restriction $PT_{scalsum} \leq 150$ GeV would lead to a good separation of the stop signal events from the top background.

Therefore, the two global variables $E_{cal-tot}$ and $PT_{scalsum}$ could also be used in addition to the cuts (11)-(13) for further reduction of the top background contribution (as well as for reduction of the QCD background). The more efficient one is $E_{cal-tot}$ which would allow us to completely separate the stop events from the top background.

[3] That is equivalent to setting a lower limit for the missing energy.

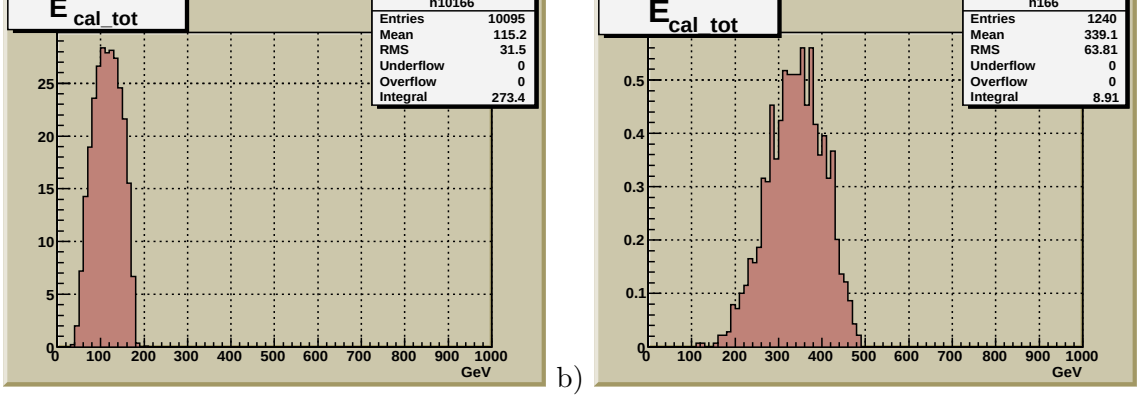

Figure 13: *Total energy $E_{cal-tot}$ distribution.* **a)** *stop pair production;* **b)** *top pair production.*

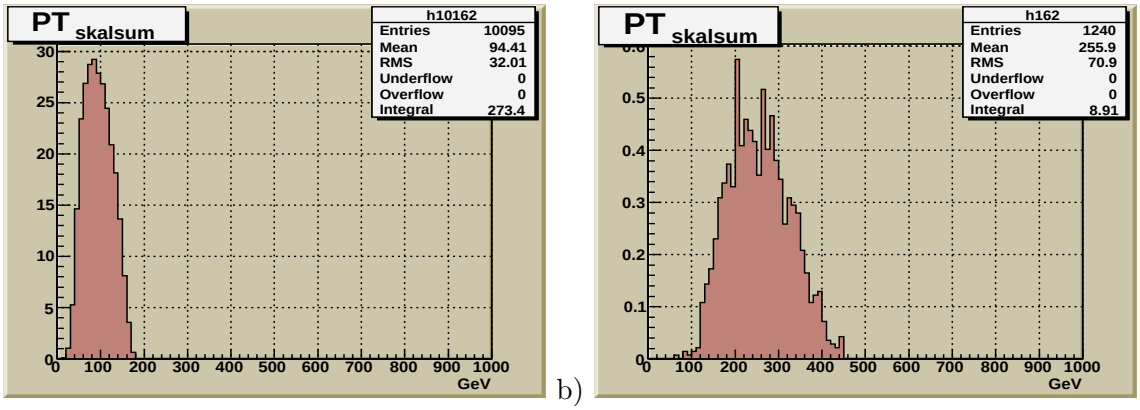

Figure 14: *$PT_{scalsum}$- distribution.* **a)** *stop pair production;* **b)** *top pair production.*

3.6 Signal–to–background ratio.

To conclude this Section, let us mention that from the "Integral" values, given in Figs.6-14, one may see that the signal–to–background ratio can be expected to be of the order $S/B = 30$. In other words, the cuts (11)-(13) would provide a sample of selected events where the signal stop events dominate over the top background by more than an order of magnitude. The contribution of the top background is reduced by these cuts down to only 8 events per year.

Finally, we present the efficiency values for the three cuts (11)-(13) as defined in subsection 3.2. We define them as the summary efficiencies. It means that if Eff_1 is the efficiency of the first cut (11), Eff_{12} is the efficiency of applying the first cut (11) and then second cut (12). Analogously, Eff_{123} is the efficiency of the successive application of the cuts (11), (12) and (13). We obtained the following results, which demonstrate the crucial importance of the cut (13) in the reduction of the top background:

- For SIGNAL STOP events :
$$Eff_1 = 0.84; \quad Eff_{12} = 0.81; \quad Eff_{123} = 0.4038;$$
- For BACKGROUND TOP events :
$$Eff_1 = 0.94; \quad Eff_{12} = 0.15; \quad Eff_{123} = 0.0012.$$

4 Distributions of the signal muons.

To select the signal stop pair production events shown in the left plot of Fig.2, one has to identify the muon from the W decay. The corresponding kinematic distributions of the signal muons are shown in Fig.15.

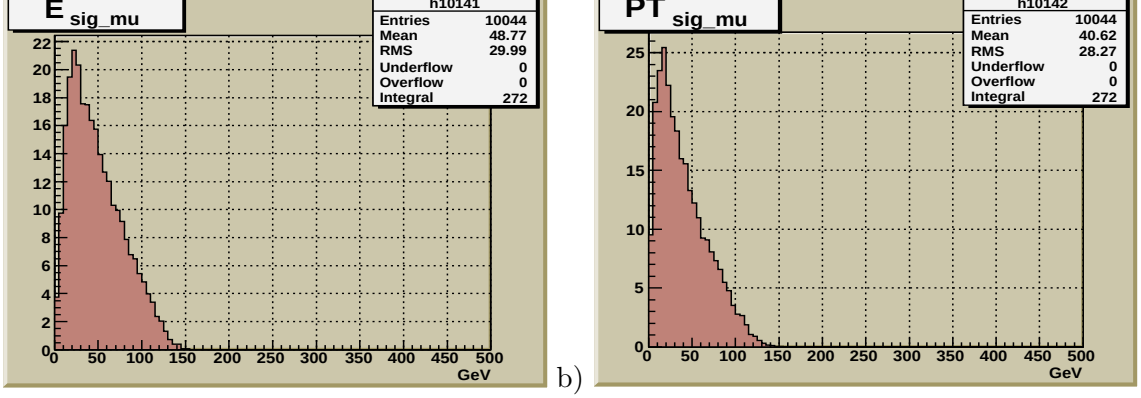

Figure 15: **a)** *Energy distributions of signal muons.* **b)** *PT distributions of signal muons.*

There are, however, muons in the event coming from leptonic and semileptonic decays of hadrons. Fig.16 **a)** and Fig.16 **b)** show the energy E_{dec-mu} and the transverse momentum PT_{dec-mu} spectra of these muons stemming from hadron decays within the detector volume (for which we took the size from TESLA TDR [5]). It can be seen that the decay muons have a rather small energy E_{dec-mu} and transverse momentum PT_{dec-mu}, their mean values are about 0.94 and 0.76 GeV, respectively. The analogous spectra for the signal muons in Fig.15 show that the signal muons have a much higher energy E_{sig-mu} and transverse momentum PT_{sig-mu}. The mean value of the signal muons energy E_{sig-mu} is about 50 times higher than the mean value of the energy of the decay muons. An analogous difference can be seen between the mean values of transverse momenta PT of signal and decay muons. One can cut off most low–energy decay muons rejecting those with $E_{mu} \leq 4$ GeV. Such a cut leads to a loss of only 0.7% of the signal events.

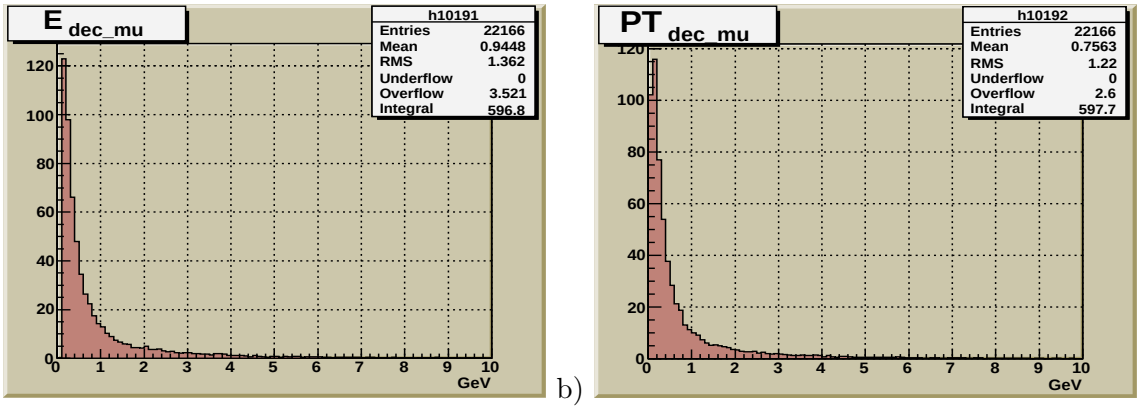

Figure 16: *Distributions of background muons.* **a)** *Energy distribution;* **b)** *PT distribution.*

We have also studied another way to select the signal muon from W decay. If the axes of all four jets in the event are known, then in general the signal muon has the largest transverse momentum with respect to any of these jet axes.

5 Optimal variables for further signal/background separation.

Let us first consider the invariant mass of the system that contains all observable objects in the final state. This invariant mass is the modulus of the vectorial sum of the 4-momenta of all four jets in an event plus the 4-momentum of the signal muon

$$M_{inv}(Alljets + \mu) = \sqrt{(\Sigma_{i=1,2,3,4} P^i_{jet} + P_\mu)^2}. \qquad (14)$$

The distribution of this invariant mass is shown in Fig.17. Plot **a)** shows the results for stop pair production while the plot **b)** is for top pair production. As seen from these plots, the cut $M_{inv}(Alljets + \mu) \leq 200$ GeV will give a good separation of signal stop and top background events.

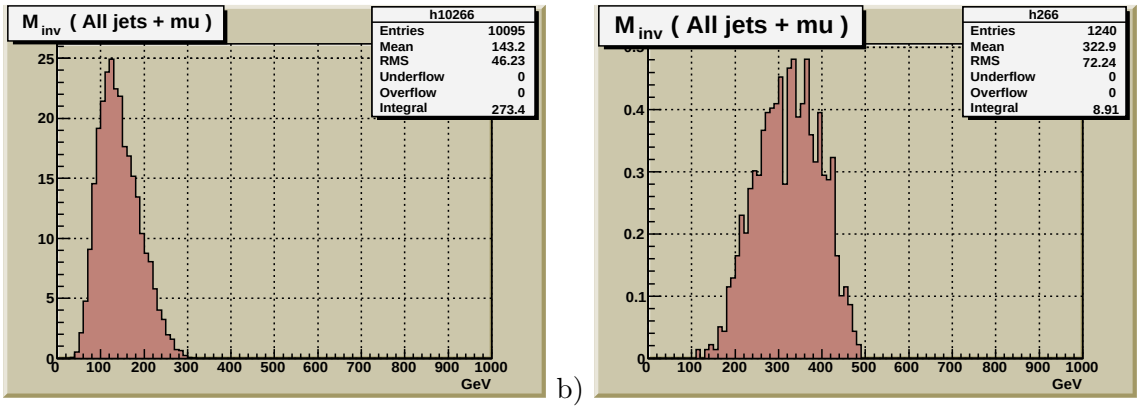

Figure 17: *Distribution of number of events versus the reconstructed invariant mass of all jets and signal muon* $M_{inv}(Alljets + \mu)$. **a)** *stop pair production;* **b)** *top pair production.*

An even more efficient separation of the signal and the background can be obtained by using the invariant mass of all jets which is the modulus of the vectorial sum of the 4-momenta of all four jets

$$M_{inv}(Alljets) = \sqrt{(\Sigma_{i=1,2,3,4} P^i_{jet})^2}. \tag{15}$$

The corresponding distribution for the signal stop events is shown in Fig.18 **a)** and for the background top events is shown in Fig.18 **b)**. Applying the cut $M_{inv}(Alljets) \leq 120$ GeV leads to a practically complete separation of signal stop and top background events. Both cuts on the invariant masses are especially useful if there is more than two years running time.

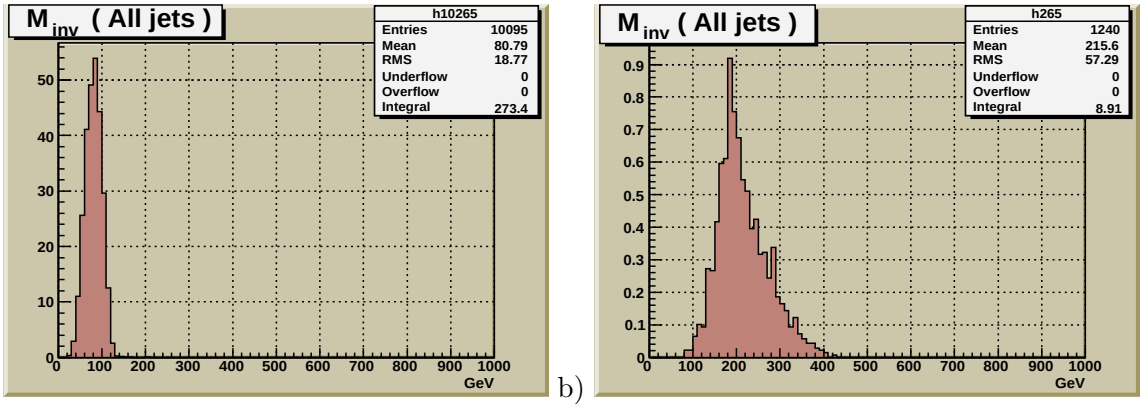

Figure 18: *Distribution of number of events versus the reconstructed invariant mass of all jets* $M_{inv}(Alljets)$. **a)** *stop pair production;* **b)** *top pair production.*

Another useful variable that can also be used for the separation of the signal and the background is the missing mass

$$M_{miss} = \sqrt{(500 - (\Sigma_{i=1,2,3,4} E^i_{jet} + E_\mu))^2 - (\Sigma_{i=1,2,3,4} P^i_{jet} + P_\mu)^2}. \tag{16}$$

Here we denote P^i_{jet} as the 3-momentum of the jet i while in all other formulae we consider P^i_{jet} as the 4-momentum. The distribution of this invariant mass is shown in Fig.19. Plot **a)** shows the results for stop pair production while the plot **b)** is for top pair production. As seen

from these plots, the cut $M_{miss} \geq 250$ GeV will give an additional separation of signal stop and top background events.

a) 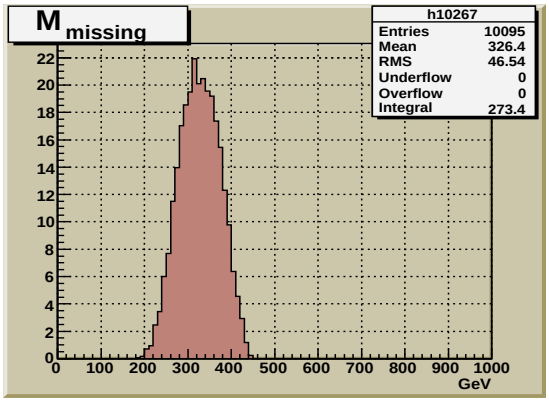

b) 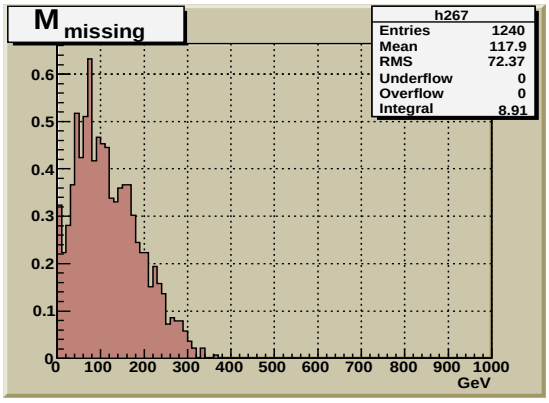

Figure 19: *Distribution of number of events versus the missing mass variable.* **a)** *stop pair production;* **b)** *top pair production.*

6 Determination of scalar top quark mass.

We first define the invariant mass $M_{inv}(b\text{-jet},JETS_W)$: [4]

$$M_{inv}(b-jet, JETS_W) \equiv M_{inv}[b-jet+(all-non-b-jets)] = \\ = \sqrt{(P_{b-jet}+P_{all-non-b-jets})^2}, \qquad (17)$$

which is constructed as the modulus of the vectorial sum of the 4-momentum $P^{\mu}_{b-jet(\bar{b}-jet)}$ of the b-jet ($\bar{b}$-jet), plus the total 4-momentum of "all-non-b-jets" system stemming from the W decay ($P^{\mu}_{all-non-b-jets} = P^{\mu}_{jet1_W} + P^{\mu}_{jet2_W}$).

This will allow us to determine the mass of the stop quark to a good accuracy. More precisely, if the signal event contains a $\mu^-(\mu^+)$ as the signal muon, we have to take the b-jet ($\bar{b}$-jet) (see Fig.2). This is only possible if one can discriminate between b- and $\bar{b}$-jets experimentally. Methods of experimental determination of the charge of the b-jet($\bar{b}$-jet) were developed in [20]. In this paper we use PYTHIA for the determination of b- and $\bar{b}$-jets. In reality, according to [20], a 50% efficiency of the separation of b-jets and 80% of the corresponding purity can be expected. It means that to get a sample of 273 signal stop events one needs about two years of ILC running for collecting the necessary statistics.

The distribution of the invariant mass of the "b-jet+(all-non-b-jets)" system in the case of stop pair production is shown in plot **a)** of Fig.20. We only used the samples of events which passed the cuts (11)-(13). This distribution has a peak at $M_{inv}(b\text{-jet},JETS_{W^*}) \approx 50$ GeV. In the case of top pair production (see the right plot of Fig.2) the invariant mass distribution of the "b-jet+(all-non-b-jets)" system shown in Fig.20 **b)** has a peak which approximately reproduces the input value of the top quark mass $M_{top} = 170.9(\pm 1.8)$ GeV (see Section 2). The accuracy is not high due to the strong suppression of the top background by the applied cuts (11)-(13). Recall that according to the "Integral" values of these plots, only about 8 top events per one year (i.e., about 3%) are expected to appear as an admixture to the stop signal. Taking into account this suppression of the top background by about two orders of magnitude, especially in the region $80 < M_{inv}(b\text{-jet}, JETS_W) < 140$ GeV, we can conclude that the $M_{inv}(b\text{-jet}, JETS_W)$ distribution also yields a good separation of signal and background events.

[4] We follow here the notations of subsection 3.1

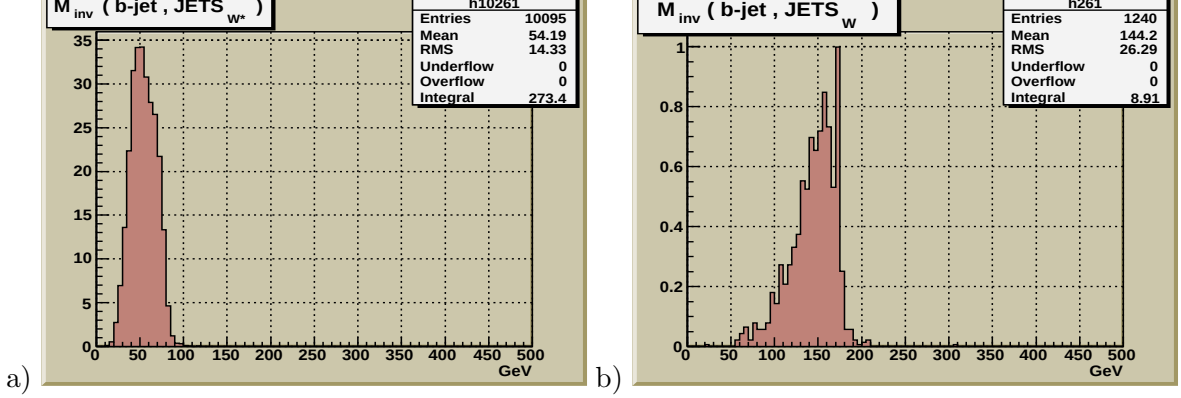

Figure 20: *The spectra of the invariant masses M_{inv}(b-jet,$JETS_W$) of the "b-jet+(all- non-b-jets)" system.* **a)** *stop pair production;* **b)** *top pair production.*

In the stop case, one has to take into account that one of the stops decays into three jets plus a neutralino $\tilde{\chi}_1^0$. Therefore, the right edge of the invariant mass distribution of the "b-jet+(all-non-b-jets)" system corresponds to the mass difference $M_{\tilde{t}_1} - M_{\tilde{\chi}_1^0}$.

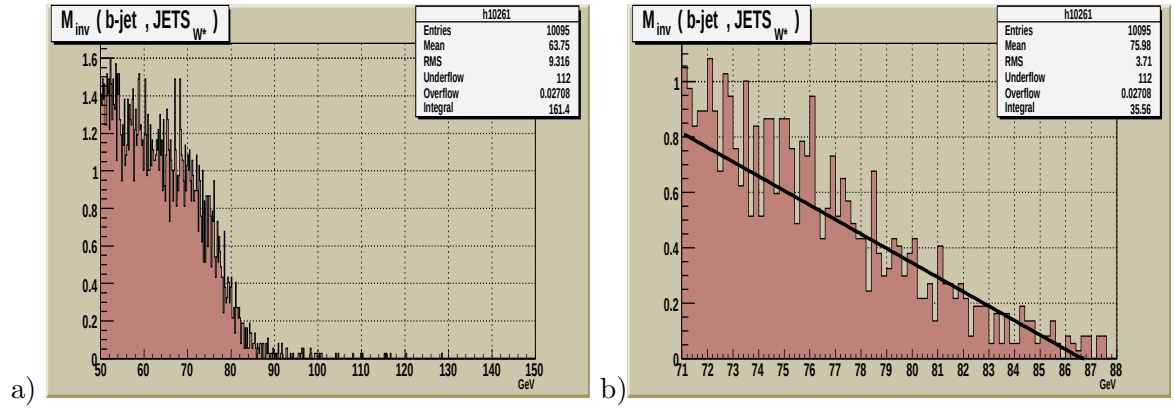

Figure 21: *Fitting the right–edge.* **a)** *zoom in of the right slopes of the analogous plots in Fig.20;* **b)** *the fitted regions.*

A linear fit to the right slope of the shown M_{inv}(b-jet,$JETS_{W^*}$) distribution is used to find its right edge, i.e. the position of its intersection with the x–axis. This also diminishes the bias due to the long tail. Plot **a)** of Fig.21, which shows in more detail the right part of Fig.20 **a)**, has a smaller binning in order to better define the slope region. Our aim is to find out that slope interval which can lead to the reconstruction of the stop mass. We have found a linear fit to the chosen slope region which is shown in Fig.21 **a)**, gives the position intersection with the x-axis: $M_{inv}^{right-edge}$(b-jet,$JETS_{W^*}$) $= 87 \pm 0.1$ GeV. Adding the mass of the neutralino $M_{\tilde{\chi}_1^0} = 80.9$ GeV one gets the reconstructed stop mass $M_{\tilde{t}_1}^{reco} = 167.9 \pm 0.1$ GeV which reproduces the input value $M_{\tilde{t}_1} = 167.9$ GeV.

The error obtained for the stop mass is so small because it is only the statistical error corresponding to the generated Monte Carlo events. The value of the "Integral" given in the Fig.21 **b)** shows that with two years statistics we may expect only about 35 selected events in the region of the slope. It would lead to a larger experimental error than that given above. A further Monte Carlo simulation taking into account detector effects would give a more realistic error.

7 Another top squark mass.

This section is to illustrate what will change if the mass of the top squark will be different from the one we have chosen. In our paper we have chosen a rather low scalar top quark mass. With increase of the stop mass the cross section of its production is falling steeply down. So, for example, for the case of $M_{\tilde{t}_1} = 200$ GeV the number of events per year is decreasing to 58.

With increase of the squark mass all the jets originating from its decay became more energetic and we can observe the shift of the jets invariant masses to higher energies. The same is valid for the constructed variables $E_{cal-tot}$ and $PT_{scalsum}$. The figures analogous to the ones presented in sections 3.5, 5 and 6, but corresponding to the $M_{\tilde{t}_1} = 200$ GeV can be seen below.

Figure 22 shows the distributions of the total energy deposited in the calorimeter $E_{cal-tot}$ in stop production (plot **a)**) and in top production (plot **b)**). The cut on the total visible energy of $E_{cal-tot} < 180$ GeV that eliminates completely the top background would cut off some part of signal events. A more appropriate cut in this case would be $E_{cal-tot} < 220$ GeV.

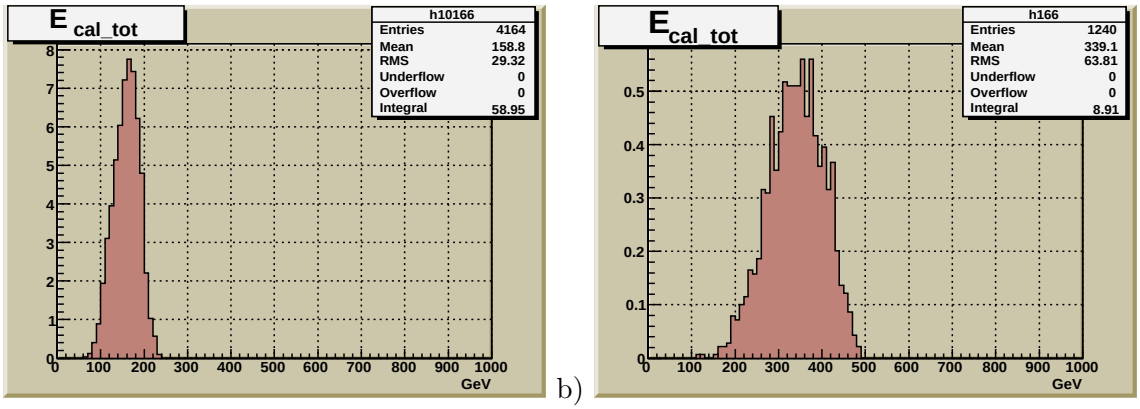

Figure 22: *Total energy $E_{cal-tot}$ distribution.* **a)** *stop pair production;* **b)** *top pair production.*

Figure 23 shows the distributions of the scalar sum of the transverse momenta of all detectable particles $PT_{scalsum} = \sum_{i=1}^{n} |PT_i|$ for the stop production (plot **a)**) and for top production (plot **b)**). The cut $PT_{scalsum} \leq 150$ GeV mentioned above would cut away some signal events. In this case, more suitable will be the cut $PT_{scalsum} \leq 180$ GeV that also helps to eliminate a big part of background.

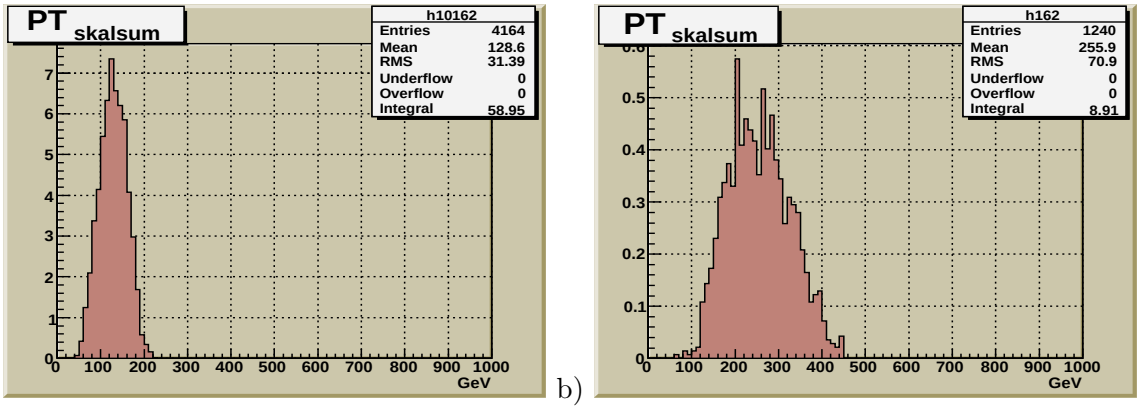

Figure 23: *$PT_{scalsum}$- distribution.* **a)** *stop pair production;* **b)** *top pair production.*

The case of the invariant mass of all observable final state objects is shown in Fig.24 (plot **a)** shows the results for stop pair production while the plot **b)** is for top pair production). Instead of the cut $M_{inv}(Alljets + \mu) \leq 200$ GeV mentioned in Section 5, a more appropriate one would be the cut $M_{inv}(Alljets + \mu) \leq 270$ GeV.

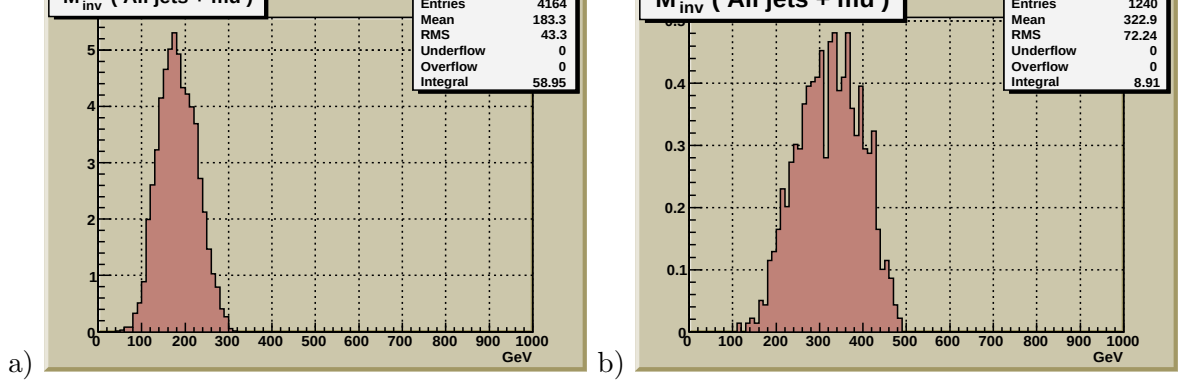

Figure 24: *Distribution of number of events versus the reconstructed invariant mass of all jets and signal muon* $M_{inv}(Alljets + \mu)$. **a)** *stop pair production;* **b)** *top pair production.*

The invariant mass of all jets $M_{inv}(Alljets)$ shown in Fig.25 (**a)** for the signal stop events and in Fig.25 **b)** for the background top events) does not give an efficient separation of the signal from the background in this case. But an additional cut $M_{inv}(Alljets) \leq 190$ GeV would still allow to kill half of the top background.

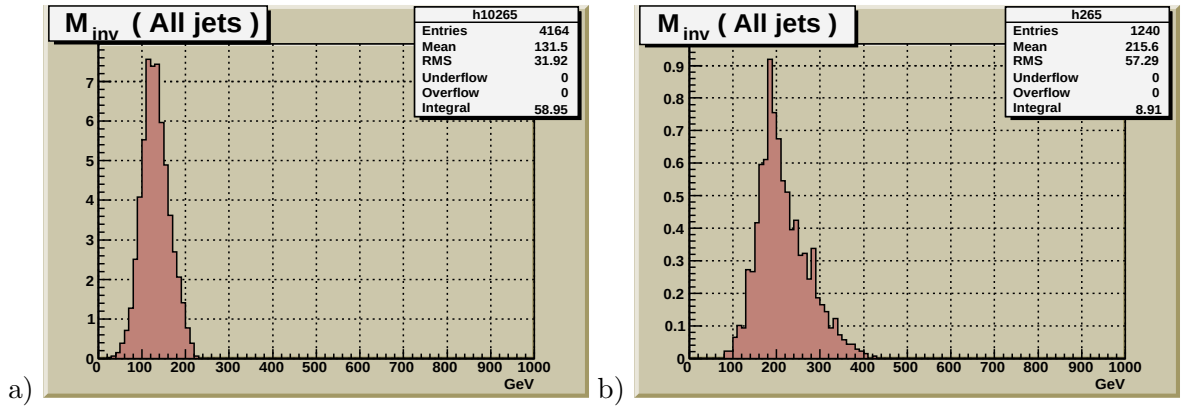

Figure 25: *Distribution of number of events versus the reconstructed invariant mass of all jets* $M_{inv}(Alljets)$. **a)** *stop pair production;* **b)** *top pair production.*

The distribution of the invariant missing mass M_{miss} shown in Fig.26 (plot **a)** is for stop pair production while plot **b)** is for top pair production) is shifted slightly to the left in comparison with the distribution presented at Fig.19 **a)**. But nevertheless, the cut $M_{miss} \geq 220$ GeV will give an additional separation of signal stop and top background events.

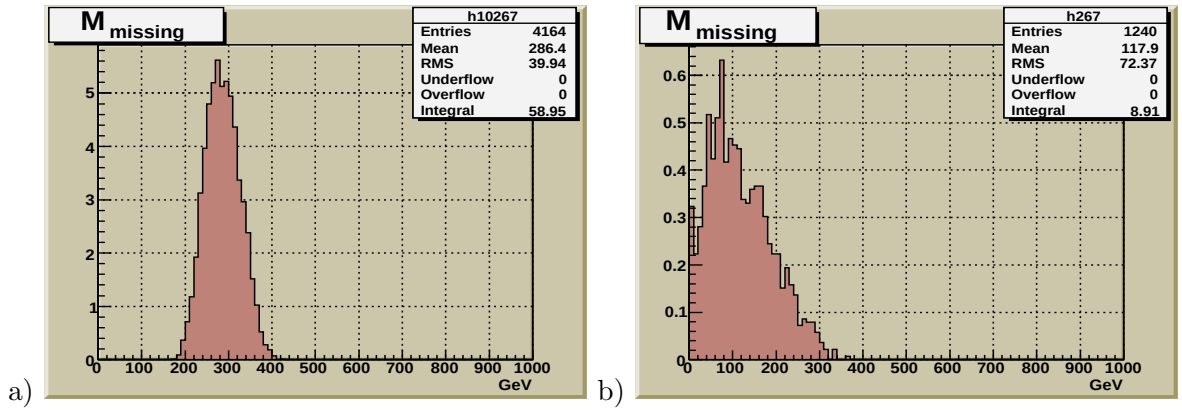

Figure 26: *Distribution of number of events versus the missing mass variable.* **a)** *stop pair production;* **b)** *top pair production.*

The distribution of the invariant mass M_{inv}(*b*-jet,$JETS_W$) of the "*b*-jet+(all-non-*b*-jets)" system in the case of stop pair production is shown in plot **a)** of Fig.27. This distribution has a peak at M_{inv}(*b*-jet,$JETS_{W^*}$) $\approx$ 80 GeV. The cut M_{inv}(*b*-jet, $JETS_W$) $<$ 130 GeV will also

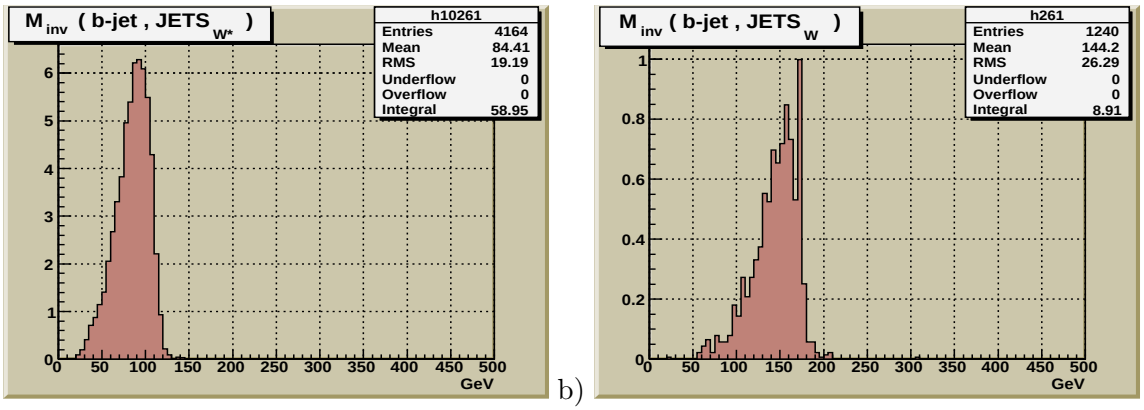

Figure 27: *The spectra of the invariant masses M_{inv}(b-jet,$JETS_W$) of the "b-jet+(all- non-b-jets)" system.* **a)** *stop pair production;* **b)** *top pair production.*

yield a good separation of signal and background events. One can also determine the mass of the stop quark following the procedure described in Section 6, but with less accuracy than in the case of the lower stop mass.

8 Conclusion.

We have studied stop pair production in electron-positron collisions within the framework of the MSSM for the total energies of the $2E^e_{beam} = \sqrt{s_{ee}} = 350$, 400, 500, 800, 1000 GeV. We assume that the stop quark decays dominantly into a chargino and a *b*-quark' $\tilde{t}_1 \to b\tilde{\chi}^{\pm}_1$, and the chargino decays into a neutralino and a W boson, $\tilde{\chi}^{\pm}_1 \to \tilde{\chi}^0_1 W^{\pm}$, where the W boson is virtual. One of the two W's decays hadronically, $W^+ \to q\bar{q}$, the other one decays leptonically, $W^- \to \mu^-\nu$.

We have performed a detailed study based on a Monte Carlo simulation with the program PYTHIA6.1 for $E^{tot}_{e+e-} = \sqrt{s_{ee}} = 500$ GeV (at this energy we expect the.highest number of the signal events for the chosen stop mass $M_{\tilde{t}_1} = 167.9$ GeV). The program CIRCE1 is used to get the parameterized spectra of electron (positron) beams taking into account the effects of beamstrahlung. PYTHIA is used to simulate stop pair production and decay as well as top pair production being the main background.

Three cuts (11)-(13) for the signal stop events have been proposed. For the separation of the signal stop events from the top background events the second cut (12) and the third cut (13) are the most important. They restrict the value of the invariant mass of the two "all-non-*b*-jets", produced in the decay of the virtual W boson, and the invariant mass of the *b*-jet. This set of cuts leads to a signal–to–background ratio as large as $S/B = 30$. Thus, we expect about 3% admixture of top events to the stop signal. This is different from the more complicated situation in stop pair production at LHC (see, for instance, [19]).

In addition, we have studied in detail various distributions of kinematic variables which can be suitable for further experimental separation of the stop signal events from the top background especially in the case of large statistics. For this purpose, we have worked out two optimal variables $M_{inv}(Alljets + \mu)$ and $M_{inv}(Alljets)$, where the latter gives practically 100% separation. A 100% separation can also be achieved with the cut $E_{cal-tot} < 180$ GeV on the total energy, deposited in the calorimeter.

We have shown that determining the end point of the distribution of the invariant mass M_{inv}(*b*-jet,$JETS_{W^*}$) of the "*b*-jet+(all-non-*b*-jets)" system allows us to measure the mass of

the stop quark with a good accuracy based on the statistics of two years running. For this the mass of χ_1^0 has to be known.

In the last Section we discussed the difference in behaviour of the main invariant distributions in the case of another stop mass $M_{\tilde{t}_1} = 200$ GeV.

In conclusion we can say that the e^+e^- channel together with the $\gamma\gamma$ channel considered in our previous Note [8] is well suited for the study of stop pair production at ILC.

9 Acknowledgements.

This work is supported by the JINR-BMBF project and by the "Fonds zur Förderung der wissenschaftlichen Forschung" (FWF) of Austria, project No.P18959-N16. The authors acknowledge support from EU under the MRTN-CT-2006-035505 and MTRN-CT-2006-503369 network programmes. A.B. was supported by the Spanish grants SAB 2006-0072, FPA 2005-01269 and FPA 2005-25348-E of the Ministero de Educacion y Ciencia.

References

[1] Y.Gol'fand and E.Likhtman, JETP Lett. 13(1971) 323;
D.Volkov and V.Akulov, Phys.Lett. B46(1973) 109;
J.Wess and B.Zumino, Nucl.Phys. B70(1974) 39.

[2] J.Ellis and S.Rudaz, Phys.Lett. B128(1983) 248.

[3] G.Altarelli and R.Rückl, Phys.Lett. B144(1984) 126;
S.Dawson, E.Eichten and C.Quigg, Phys.Rev. D31(1985) 1581;
K.Hikasa and M.Kobayashi, Phys.Rev. D36(1987) 742;
M.Drees and K.Hikasa, Phys.Lett. B252(1990) 127;
J.Ellis, G.L.Fogli and E.Lisi, Nucl.Phys. B393(1993) 3.

[4] D0 Collab., V.M. Abazov et al., Phys.Lett. B645 (2007) 119.

The CDF Collaboration, T. Aaltonen et al., Phys.Rev. D76, 072010 (2007).

[5] J.A. Aguilar-Saavedra, et al. "TESLA Technical Design Report", PART III:
Editors: R.D.Heuer, D.Miller, F.Richard, P.Zerwas. DESY, 2001;
arXiv:hep-ex/0106315.

[6] ILC Reference Design Report, v.1 "Executive Summary",
Editors: J.Brau, Y.Okada, N.Walker, 2007;
http://www.linearcollider.org/cms/?pid=1000025.

[7] ILC Reference Design Report, v.2 "Physics at the ILC",
Editors: A.Djouadi, J.Lykken, K.Mönig, Y.Okada, M.Oreglia, S.Yamashita, 2007;
http://www.linearcollider.org/cms/?pid=1000025.

[8] A.Bartl, K.Mönig, W.Majerotto, A.Skachkova, N.Skachkov,
"Pair Production of Scalar Top Quarks in Polarized Photon-Photon Collisions at ILC",
ILC-NOTE-2007-036, arXiv:0804.1700[hep-ph]

[9] A.Bartl, H.Eberl, S.Kraml, W.Majerotto and W.Porod, EPJ C2(2000)6;
hep-ph/0002115.

[10] A.Bartl, K.Moenig, W.Majerotto, A.Skachkova, N.Skachkov,
"Stop pair production in polarized photon-photon collisions",

Proc. of the Intern. Conf. on Linear Colliders (LCWS 2004), vol.II, p.919, April 19-23, 2004, Le Carre des Sciences, Paris, France.

[11] A.Finch, H.Nowak and A.Sopczak, hep-ph/0211140.

[12] M.Carena et.al, Phys.Rev. D72:115008, 2005; hep-ph/0508152.

[13] A. Sopczak et.al, hep-ph/0605225.

[14] T. Sjöstrand, P. Edén, C. Friberg, L.Lönnblad, G. Miu, S. Mrenna and E. Norrbin, Computer Phys. Commun. 135 (2001) 238.

[15] T. Ohl, "$\kappa\iota\rho\kappa\eta$ Version 1.0: Beam Spectra for Simulating Linear Collider Physics", hep-ph/9607454.

[16] J.F.Gunion, H.E.Haber, Nucl.Phys. B272(1986)1; B278(1986)449; Erratum B402(1993)567.

[17] E. Brubaker et al. "Combination of CDF and D0 results on the mass of the top quark"; By Tevatron Electroweak Working Group, Fermilab-TM-2380-E, 19 Mar2007; arXiv:hep-ex/0703034.

[18] R.Hawkings, "Vertex detector and flavour tagging studies for TESLA liear collider", LC-PHSM-2000-021, 2000

[19] U.Dydak, "Search for the stop quark with CMS at the LHC"; CMS TN/96-022, CERN, 1996;
U.Dydak, H.Rohringer and J.Tuominiemi, "Study of the channel gluino → stop + top", CMS TN/96–103, CERN, 1996.

[20] C.J.S.Damerell, D.J.Jackson, eConf960625 (1996) DET078;
R.Hawkings, LC-PHSM-2000-021;
S.M.Xella Hansen, D.J.Jackson, R.Hawkings, C.J.S.Damerell, LC-PHSM-2001-024;
S.M.Xella Hansen, M.Wing, D.J.Jackson, N. De Groot, C.J.S.Damerell, LC-PHSM-2003-061;
S.M.Xella Hansen et al. [Linear Collider Flavour Identification Collaboration], Nucl.Instrum.Meth.A501,106(2003); S.Hillert, C.J.S.Damerell, eConf0508141 (2005) ALCPG 1403.

[21] G.Moortgat-Pick et.al., "The role of polarized positrons and electrons in revealing fundamental interactions at the Linear Collider", hep-ph/0507011.

[22] D.Shulte, Ph.D.thesis; K.Yokoya and P.Chen, KEK Preprint 91-2, April 1991;
http://www-sldnt.slac.stanford.edu/nlc/programs/guinea_pig/gp_index.html.